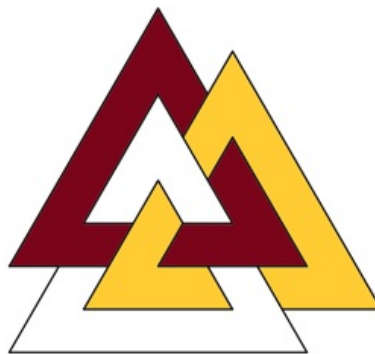


# Applications of Signatures in Diagnosing Breast Cancer

Anna Grim and Chehrzad Shakiban

University of St. Thomas



The Minnesota Journal of Undergraduate Mathematics

Volume 1 Number 1 (2015)

---

The Minnesota Journal of Undergraduate Mathematics

Volume 1 Number 1 (2015)

# Applications of Signatures in Diagnosing Breast Cancer

Anna Grim\* and Chehrzad Shakiban

University of St. Thomas

**ABSTRACT.** Noninvasive diagnosis of breast tumors persists as a challenge in oncology because the structural differences between benign and malignant tumors are indistinguishable to the human eye. However, the application of signature curve symmetry can diagnose tumors by mathematically analyzing curvature. Our methodology quantifies a two-dimensional (2D) tumor contour by the rigidly invariant signature curve parametrization taken with respect to arc length. The differing shape of benign and malignant tumors results in contrasting global and local symmetry patterns in the signature curve. Benign tumors are distinctive by a high degree of global symmetry in the 2D tumor contour, whereas, malignant tumors exhibit multiple types of local symmetry embedded within their signature curve. The methodology has been implemented on over 150 tumors, demonstrating a statistically significant correlation between curvature complexity and malignancy.

## 1. INTRODUCTION

**1.1. Biological Background.** Although tumors are detected by mammograms, diagnosis cannot be ascertained because benign and malignant tumors can be visually indistinct. Despite malignant tumors having a more irregularly shaped contour, its degree of complexity is a subjective assessment and unreliable for official diagnosis [17]. Thus, surgical incision and histological examination of the tumor is the standard procedure for accurate diagnosis. However, the high volume of mammograms performed each year increases the risk of over diagnosis and unnecessary procedures by approximately 30% [20]. Our methodology presents a solution by providing an objective assessment of tumors detected on mammograms by analyzing tumor morphology with signature curves.

Differing cellular growth patterns and tumor encapsulation instigate the contrasting morphology between benign and malignant tumors [20]. Initially, benign tumors grow acutely, but the growth stabilizes with a fastidious cellular metabolism [22]. In contrast, malignant tumors develop with an unstable growth engendered by a chaotic cellular metabolism [22]. The morphology of a malignant tumor differentiates itself from benign tumors due to its lack of encapsulation. Benign tumors are fully enclosed within a capsule, which maintains a closed system where cellular content is uniformly dispersed in order to

---

\* *Corresponding author*

maintain a pressure equilibrium. As a result, the tumor grows as an expanding ellipsoid, which appears as an elliptical contour on a mammogram [16]. In contrast, uncoordinated cellular growth and lack of encapsulation result in finger-like proliferations on the surface of malignant tumors called spiculation [8]. Spiculation causes malignant tumors to have an irregular shape when detected on a mammogram [6]. The polar morphology of benign and malignant tumors is amplified by the signature curve where contrasting signature curve complexity and symmetry patterns can infer diagnosis.

**1.2. Signature Curves.** Signature curves are a fundamental component of our tumor diagnosis methodology due to their invariant properties in the Euclidean plane [10]. The signature curve  $S$  of a 2D contour is the parametrization such that  $S = \{(\kappa(t), \kappa_s(t))\}$ , where  $\kappa$  is curvature and  $\kappa_s$  is the derivative of curvature. A theorem by Élie Cartan states that

**Theorem 1.1.** *If the signature curves of two suitably non-degenerate contours are identical, then the contours must be equivalent [3, 4].*

Since curvature is invariant under rigid motions in the Euclidean plane, then the signature curve is also rigidly invariant. Therefore, the orientation of the contour is independent of the resulting signature curve.

In order to calculate the signature curve, consider a parametrized curve  $C = \{(x(t), y(t))\}$  in the Euclidean plane so that  $C \subset E \simeq \mathbb{R}^2$  [13]. The signature curve is obtained by calculating the curvature and derivative of curvature along the curve  $C$ . According to [1] and [2], the approximate curvature  $\tilde{\kappa}$  at an arbitrary point  $P_i \in C$  with respect to arc length is obtained by choosing points  $P_{i-1}, P_{i+1} \in C$ , forming the triangle illustrated in Figure 1. Let  $\Delta$  represent the signed area of the triangle formed by  $P_{i-1}, P_i, P_{i+1}$  and  $s$  be the semi-perimeter, so that using Heron's formula we have  $\Delta = \pm \sqrt{s(s-a)(s-b)(s-c)}$  and  $s = \frac{1}{2}(a+b+c)$  [1]. The curvature at  $P_i$  is calculated by using the formula,

$$\tilde{\kappa}(P_{i-1}, P_i, P_{i+1}) = 4 \frac{\Delta}{abc} = \pm 4 \frac{\sqrt{s(s-a)(s-b)(s-c)}}{abc}. \quad (1)$$

The derivative of curvature is calculated in a similar manner by calculating the approximate curvature at the points  $P_{i-1}, P_{i+1} \in C$  so that the approximate derivative of curvature  $\tilde{\kappa}_s$  at point  $P_i$  can be calculated as

$$\tilde{\kappa}_s(P_{i-2}, P_{i-1}, P_i, P_{i+1}, P_{i+2}) = \frac{\tilde{\kappa}(P_i, P_{i+1}, P_{i+2}) - \tilde{\kappa}(P_{i-2}, P_{i-1}, P_i)}{\mathbf{d}(P_{i+1}, P_{i-1})}, \quad (2)$$

where  $\mathbf{d}(P_{i+1}, P_{i-1})$  is the Euclidean distance between  $P_{i+1}$  and  $P_{i-1}$ . Equations (1) and (2) are used to obtain the signature curve parametrization  $S$ , such that

$$S = \{\tilde{\kappa}(P_{i-1}, P_i, P_{i+1}), \tilde{\kappa}_s(P_{i-2}, P_{i-1}, P_i, P_{i+1}, P_{i+2})\}.$$

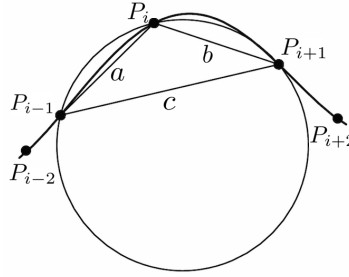


FIGURE 1. Approximate curvature at an arbitrary point

**1.3. Symmetry of Signature Curves.** Signature curves amplify the curvature complexity of a contour and accentuate global and local symmetry patterns. For example, a symmetrical contour such as an ellipse has a double overlapping signature curve due to the reflective *global contour symmetry*.

**Definition 1.2.** *Global contour symmetry* is a closed contour with a bilateral axis of symmetry.

Although global symmetry could also include rotational, reflectional and translational symmetry, this research study is strictly focused on quantifying reflectional global symmetry. Contours that are globally symmetrical result in signature curves that are globally signature. Thus, we also define:

**Definition 1.3.** *Global signature symmetry* is a signature curve with a bilateral axis of symmetry at the  $\kappa$ - or  $\kappa_s$ -axis.

In the application of breast tumors, benign tumors display global contour and signature symmetry because their 2D contours are generally elliptical. However, malignant tumors lack global symmetry due to their irregular shape, but spiculation creates small symmetrical regions within the contour resulting in *local symmetry*. Signature curves detect local symmetry as signature segments that are symmetrical across either the  $\kappa$ - or  $\kappa_s$ -axis. Spiculation leads to two types of local symmetry called local individual and joint symmetry, which we have defined based on our findings. We introduce the following:

**Definition 1.4.** *Local individual symmetry* is a signature segment with a bilateral axis of symmetry.

The axis of symmetry perpendicularly passes through the midpoint of the horizontal axis connecting the initial and final points of the signature segment; as seen in Figure 2. In application, a single spiculation creates an individually symmetrical segment on the signature curve. We also define *local joint symmetry* to be defined as

**Definition 1.5.** *Local joint symmetry* is a reflective symmetry between two distinct signature segments.

The axis of symmetry is equidistant from the segments and perpendicular to the horizontal axis connecting the initial and final points of both signature segments; as seen in Figure 3.

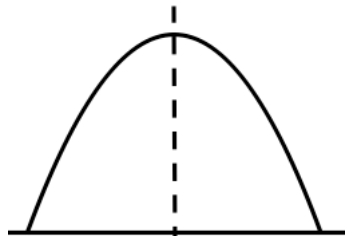


FIGURE 2. Local Individual Symmetry

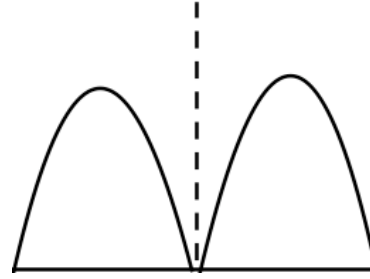


FIGURE 3. Local Joint Symmetry

We will proceed by describing the methodology for each symmetry measure and following up with the results obtained from our data set. In Section 2, we describe the following methodologies of zero curvature points in 2.1, global symmetry in 2.2, and local symmetry in 2.3. In Section 2.2, we will outline both methods of calculating global symmetry, which include global contour symmetry in 2.2.1 and global signature symmetry in 2.2.2 with the follow up results in Section 3.3. In Section 2.3, we will describe our local symmetry methodologies for local individual symmetry in 2.3.1 and local joint symmetry in 2.3.2 with the follow up results in Section 3.4.

## 2. METHODOLOGY

**2.1. Zero Curvature Points.** In this research study, let *zero curvature points* denote points along the contour where either  $\kappa(t) = 0$  or  $\kappa_s(t) = 0$ . Although the term *zero curvature points* seems to exclude the set of points where  $\kappa_s(t) = 0$ , we will use this terminology to include both sets of points. Zero curvature points were identified by detecting a change in sign of  $\kappa(t)$  or  $\kappa_s(t)$  caused by  $S$  crossing the  $\kappa$ - or  $\kappa_s$ -axis. The range  $R$  of zero curvature points on each respective axis is  $R_\kappa = \max\{\kappa_s(t)\} - \min\{\kappa_s(t)\}$ , where  $\kappa(t) = 0$ , and  $R_{\kappa_s} = \max\{\kappa(t)\} - \min\{\kappa(t)\}$ , where  $\kappa_s(t) = 0$ . The density of zero curvature points on each axis is calculated as,

$$\rho_\kappa = \frac{R_\kappa}{\eta_{\kappa_s}} \quad \text{and} \quad \rho_{\kappa_s} = \frac{R_{\kappa_s}}{\eta_\kappa},$$

where  $\eta$  is the number of zero curvature points on the respective axis.

**2.2. Global Symmetry.** A benign contour is approximately globally symmetrical with several axes of symmetry as seen in Figure 4. The contour's corresponding signature in Figure 5 has a nearly double overlapping signature curve due to the global symmetry. Therefore, we developed two methods referred to as global contour and signature symmetry.

**2.2.1. Global Contour Symmetry.** For a given contour, the set of points is translated so that the contour's center of mass is coincident with the origin. At the beginning of each symmetry calculation iteration, the contour is rotated  $\Delta\theta = \frac{5\pi}{180}$  radians and points are divided by the  $x$ -axis into  $C^\alpha$  and  $C^\beta$ . The rotation increment  $\Delta\theta$  was selected because it is relatively "small" and computationally efficient.  $C^\alpha$  is defined as the set of all  $\{(x(t), y(t))\} \in C$

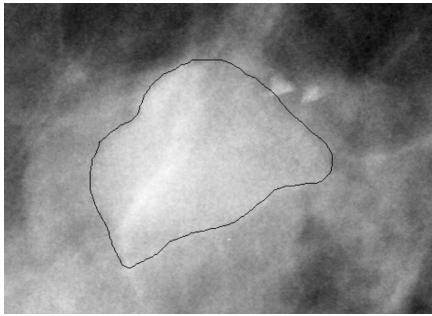


FIGURE 4. Benign Tumor Contour

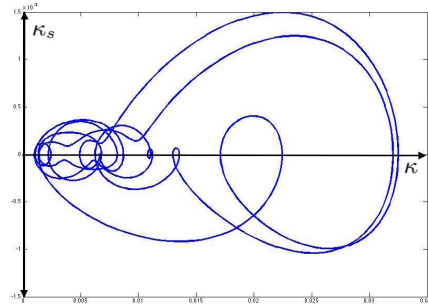


FIGURE 5. Signature Curve

such that  $y(t) < 0$  and  $C^\beta$  is the set of all  $\{(x(t), y(t)) \in C$  such that  $y(t) > 0$ , hence

$$C^\alpha = \{(x^\alpha(t), y^\alpha(t))\} \quad \text{and} \quad C^\beta = \{(x^\beta(t), y^\beta(t))\}. \quad (3)$$

For  $m$  points in  $C^\alpha$  and  $n$  points in  $C^\beta$ , the cumulative magnitudes  $\|v^\alpha\|$  and  $\|v^\beta\|$  are calculated, respectively. Although we could cumulate the distribution by using the first point as our initial point and continuing successively, this can be problematic if, for example, the first point is an outlier. To circumvent this scenario, we will reorder the distributions so that the centroid is the initial point and each successive point alternates between the left and right side of the centroid. So now we have distributions with nontrivial ordering and will proceed to cumulate the distributions by calculating the cumulative distance magnitude of each point. The cumulative magnitude is recursively defined, where the magnitude of a point is added to the summation of all preceding point's magnitudes, such that an arbitrary  $\|v_i^\alpha\|$  is

$$\|v_i^\alpha\| = \sqrt{(x_i^\alpha(t))^2 + (y_i^\alpha(t))^2} + \sum_{m=0}^{i-1} \|v_m^\alpha\|.$$

The magnitudes are compiled into a vector  $\hat{v}$ , where the magnitudes from  $\|v^\alpha\|$  are negated and  $\hat{v}$  follows as

$$\hat{v} = (-\|v_0^\alpha\|, \dots, -\|v_m^\alpha\|, \|v_0^\beta\|, \dots, \|v_n^\beta\|).$$

The symmetry of the distribution  $\hat{v}$  is quantified by calculating skewness  $\delta$  using the formula,

$$\delta = \frac{\frac{1}{m+n} \sum_{p=1}^{m+n} v_p^3}{\left( \frac{1}{m+n} \sum_{p=1}^{m+n} v_p^2 \right)^{3/2}}. \quad (4)$$

The symmetry algorithm is repeated for 37 iterations for each of the  $\Delta\theta = \frac{5\pi}{180}$  rotations of the contour through  $\theta \in [0, \pi]$ .

**2.2.2. Global Signature Symmetry.** At the beginning of each symmetry calculation iteration, the contour is rotated  $\Delta\theta = \frac{5\pi}{180}$  radians and points are divided as in equation (3). The signature curve of both  $C^\alpha$  and  $C^\beta$  is calculated so that  $S^\alpha = \{\kappa^\alpha(t), \kappa_s^\alpha(t)\}$  and  $S^\beta =$

$\{\kappa^\beta(t), \kappa_s^\beta(t)\}$ . For  $m$  points in  $S^\alpha$  the magnitude  $\|u^\alpha(t)\|$  and magnitude  $\|u^\beta(t)\|$  of  $n$  points in  $S^\beta$  is calculated such that an arbitrary magnitude is

$$\|u_i^\alpha(t)\| = \sqrt{(\kappa_i^\alpha(t))^2 + (\kappa_{s_i}^\alpha(t))^2}.$$

The magnitudes are compiled into a vector  $\hat{u}$ , where the magnitudes from  $\|u^\alpha\|$  are negated so that

$$\hat{u} = (-\|u_0^\alpha\|, \dots, -\|u_m^\alpha\|, \|u_0^\beta\|, \dots, \|u_n^\beta\|).$$

The symmetry of the distribution  $\hat{u}$  is quantified by calculating skewness  $\delta$  with equation (4). The symmetry algorithm is repeated for 37 iterations for each of the  $\Delta\theta = \frac{5\pi}{180}$  rotations of the contour through  $\theta \in [0, \pi]$ .

**2.3. Local Symmetry.** The signature curve of a malignant contour is symmetrical across both the  $\kappa$ - and  $\kappa_s$ -axis as seen in Figure 7. The local symmetry is due to a significant amount of spiculation around the malignant tumor contour as seen in Figure 6. Thus, local joint and individual symmetry were quantified with respect to each axis using the symmetry algorithm.

**2.3.1. Local Individual Symmetry.** For individual symmetry,  $S$  is segmented by the  $\kappa$ -axis so that  $\kappa_s(t) = 0$  only at the initial and final points of a segment  $L$ . First, we let the point  $(x_c, y_c)$  be the midpoint of our signature segment, so that it lies on the bilateral axis dividing the signature segment. Let  $L^\alpha$  be the set of all  $(\kappa(t), \kappa_s(t)) \in L$  such that  $\kappa(t) < x_c$  and  $L^\beta$  be the set of all  $(\kappa(t), \kappa_s(t)) \in L$  such that  $\kappa(t) > x_c$ , where

$$L^\alpha = \{(\kappa^\alpha(t), \kappa_s^\alpha(t))\} \quad \text{and} \quad L^\beta = \{(\kappa^\beta(t), \kappa_s^\beta(t))\}. \quad (5)$$

For all points in  $L^\alpha$  and  $L^\beta$ , the cumulative distance between each point and the midpoint are calculated so that for an arbitrary point the cumulative distance  $\|v_i^\alpha\|$  is

$$\|v_i^\alpha\| = \sqrt{(\kappa_i^\alpha(t) - x_m)^2 + (\kappa_{s_i}^\alpha(t) - y_m)^2} + \sum_{m=0}^{i-1} \|v_m^\alpha\|. \quad (6)$$

The magnitudes are compiled into a vector  $\hat{v}$  as previously described and the symmetry of the distribution is calculated with equation (4). This process is repeated and adapted appropriately for when  $S$  is segmented by the  $\kappa_s$ -axis.

**2.3.2. Local Joint Symmetry.** For local joint symmetry,  $S$  is segmented by the  $\kappa$ -axis so that  $\kappa_s(t) = 0$  at only the initial and final point of a segment  $L$ . Two distinct segments  $L^\alpha$  and  $L^\beta$  are selected from  $S$ , then translated so that they are aligned as in Figure 3 with  $(x_c, y_c)$  as the point where the segments are coincident. The symmetry calculation between the two segments is equivalent to the process described in equations (5) and (6) so the skewness can be calculated as in equation (4). The process described is repeated and adapted appropriately for when  $S$  is segmented by the  $\kappa_s$ -axis.

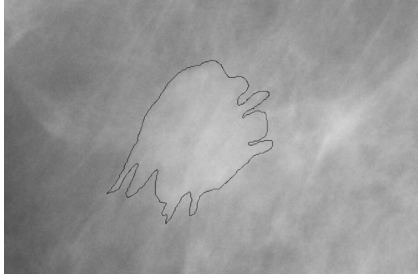


FIGURE 6. Malignant Tumor Contour

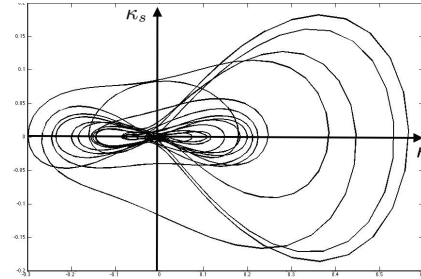


FIGURE 7. Signature Curve

### 3. RESULTS

**3.1. Data Set.** The data set contains 78 benign and 78 malignant mammograms diagnosed by expert radiologists. Atypical tumors comprise approximately 10% of the data set with seven spiculated benign and nine circumscribed malignant tumors. An atypical benign tumor contains spiculations, whereas an atypical malignant tumor lacks spiculations. The data set was downloaded from the University of South Florida Digital Database for Screening Mammography and the Mammographic Image Analysis Society [19, 21]. Each image is between  $512 \times 512$  and  $1024 \times 1024$  pixels that were originally acquired from either a Lumysis or Howtek scanner [21]. All of the tumors from both databases included an official diagnosis and delineation of the tumor contour drawn by a radiologist. After downloading the images, each image was individually discretized into a set of  $(x, y)$  points using active contour segmentation [11, 12].

**3.2. Zero Curvature Points.** The results for typical versus atypical tumors are included in Table 1, where each value is the mean  $\pm$  standard deviation. The following abbreviations have been used in the table, “A” and “T” indicate atypical and typical, while “B” and “M” indicate benign and malignant. Based on the results in Table 1, signature curves with a wide range and high number of zero curvature points represent a malignant contour because the curvature is frequently changing. In contrast, benign contours have fewer zero curvature points and smaller ranges because the curvature is relatively constant.

	$\kappa(t)=0$	$\kappa_s(t)=0$	$R_\kappa$	$R_{\kappa_s}$	$\rho_\kappa$	$\rho_{\kappa_s}$
TB	$3.66 \pm 3.29$	$16.0 \pm 3.97$	$0.06 \pm 0.06$	$0.02 \pm 0.03$	$0.004 \pm 0.004$	$0.004 \pm 0.006$
AB	$28.8 \pm 11.0$	$46.3 \pm 20.5$	$2.94 \pm 6.57$	$6.57 \pm 10.2$	$0.08 \pm 0.11$	$0.30 \pm 0.58$
TM	$28.8 \pm 10.2$	$46.3 \pm 14.8$	$1.32 \pm 1.59$	$1.96 \pm 3.94$	$0.08 \pm 0.03$	$0.30 \pm 0.04$
AM	$24.2 \pm 11.9$	$41.1 \pm 15.1$	$1.13 \pm 1.23$	$1.87 \pm 2.56$	$0.02 \pm 0.04$	$0.06 \pm 0.11$

TABLE 1. Zero Curvature Point Results

**3.3. Global Symmetry.** The global contour symmetry algorithm is performed for 37 iterations for each of the  $\Delta\theta = \frac{5\pi}{180}$  rotations, where the output is a skewness value. Based on data observation, a *symmetrical axis*  $\lambda_1$  is defined as  $\delta < 0.01$  and a *very symmetrical axis*  $\lambda_2$  is defined as  $\delta < 0.001$ . A symmetry score  $\Lambda$  is calculated for each contour where

$$\Lambda = \sum \lambda_1 + \sum \lambda_2. \quad (7)$$

The results for typical versus atypical tumors is included in Table 2, where each value is the mean  $\pm$  standard deviation. Based on the results in Table 2, benign tumors have a significantly higher number of axes of symmetry. In the global contour symmetry method, 41.86% of the benign axes and 13.79% of the malignant axes meet the symmetry criteria.

In the global signature symmetry method, a *symmetrical axis*  $\lambda_1$  is defined as  $\delta < 0.3$ , a *very symmetrical axis*  $\lambda_2$  is defined as  $\delta < 0.1$ , and symmetry score is calculated with equation (7). In the global signature symmetry method, 22.04% of the benign axes and 8.489% of the malignant axes meet the symmetry criteria. The results for typical versus atypical tumors are included in Table 2, where each value is the mean  $\pm$  standard deviation.

**3.4. Local Symmetry.** In both the local individual and joint symmetry, a *symmetrical axis*  $\lambda_1$  is defined as  $\delta < 0.3$ , a *very symmetrical axis*  $\lambda_2$  is defined as  $\delta < 0.1$ . The total symmetry score is calculated by summing the local individual and joint symmetry score using equation (7). Based on the results in Table 3, malignant tumors have a higher degree of local symmetry. Spiculations result in local individual symmetry and similar spiculations on the contour result in local joint symmetry.

Contour Method	Mean $\Lambda$	Mean $\delta$
Typical Benign	17.71 $\pm$ 8.89	2.57 $\pm$ 3.15
Atypical Benign	5.06 $\pm$ 5.63	6.67 $\pm$ 5.43
Typical Malignant	0.10 $\pm$ 0.06	0.48 $\pm$ 0.28
Atypical Malignant	0.33 $\pm$ 0.17	0.29 $\pm$ 0.14
Signature Method	Mean $\Lambda$	Mean $\delta$
Typical Benign	12.07 $\pm$ 15.3	0.96 $\pm$ 0.71
Atypical Benign	0	5.99 $\pm$ 5.79
Typical Malignant	4.52 $\pm$ 8.69	2.85 $\pm$ 3.27
Atypical Malignant	0	4.34 $\pm$ 3.78

TABLE 2. Global Symmetry

$\mathcal{K}$ -axis	Mean $\lambda_1$	Mean $\lambda_2$
Typical Benign	2.55 $\pm$ 2.34	0.90 $\pm$ 0.96
Atypical Benign	5.06 $\pm$ 5.63	7.57 $\pm$ 3.10
Typical Malignant	21.25 $\pm$ 8.04	8.36 $\pm$ 4.61
Atypical Malignant	17.11 $\pm$ 9.96	6.67 $\pm$ 4.92
$\mathcal{K}_s$ -axis	Mean $\lambda_1$	Mean $\lambda_2$
Typical Benign	1.97 $\pm$ 1.47	0.55 $\pm$ 0.63
Atypical Benign	9.86 $\pm$ 5.81	2.43 $\pm$ 1.72
Typical Malignant	8.81 $\pm$ 4.37	2.83 $\pm$ 1.82
Atypical Malignant	8.00 $\pm$ 3.64	2.33 $\pm$ 2.06

TABLE 3. Local Individual Symmetry

**3.5. ROC Analysis.** We calculated an receiver operating characteristic (ROC) curve, which is a plot of the true positive rate against the false positive rate. The area under the ROC curve indicates the accuracy of our methodology to correctly diagnose benign and malignant tumors. In Figure 8, the sensitivity and specificity refer to the true positive and false positive rate, respectively. The measure is an objective assessment of the accuracy of our algorithms and objectively compares our methodology against existing automated algorithms. In our zero curvature point analysis, we combined the frequency, range, and density for the diagnosis of a given tumor. Similarly, we also combined local individual, local joint, and global contour symmetry for our symmetry algorithm.

We decided to combine measures in each methodology because we obtain a more reliable and accurate diagnosis. Our results showed that the zero curvature point analysis, global contour symmetry, and global contour symmetry have ROC analysis values of 0.8565, 0.9352, and 0.9348 respectively. Although our zero curvature point analysis has less reliable success, our symmetry algorithm is very effective and more accurate than existing methods. In a paper by Rangayyan and Nguyen, 1D and 2D ruler box counting fractal dimension were used, but only obtained ROC curve values ranging from 0.83-0.89

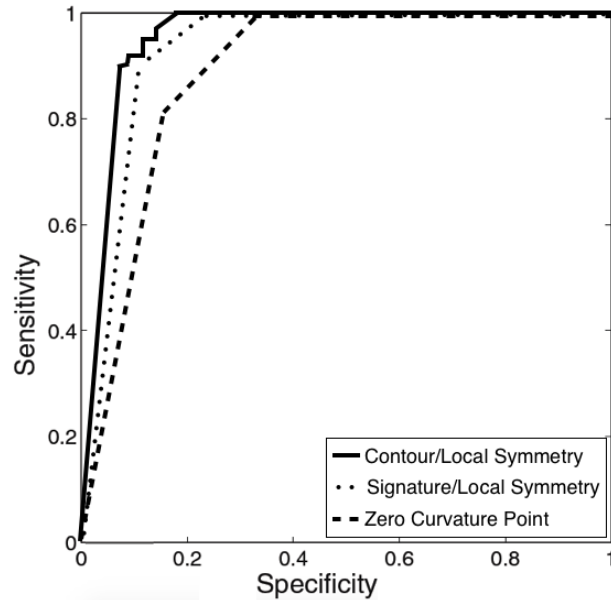


FIGURE 8. ROC Analysis

[18]. In addition, they also developed algorithms using compactness, fractional concavity, spiculation index, and a Fourier-descriptor-based factor, which obtained ROC curve values ranging from 0.77-0.93 [18]. Another study by Chen, Chung, and Hun used fractal features in an image processing texture analysis using fractals, where they obtained an ROC curve value of 0.88 [5]. In the automated diagnosis literature, we have found our symmetry algorithm to be more accurate than existing methodologies.

#### 4. DISCUSSION

Both global signature and contour symmetry were included in this study because they achieved remarkable results and present alternative methods of quantifying global symmetry. Global signature symmetry is a memoryless technique because the order of the magnitudes does not affect the symmetry value  $\delta$ . This is a problem because two dissimilar contours with identical sorted magnitude distributions could be detected as symmetrical. Although the technique successfully detects symmetry, the methodology could be improved by also quantifying angular symmetry. Also it should be noted that the cumulative magnitude method could not be used because the points along the signature curve are not uniformly spaced with respect to arc length.

In global contour symmetry, each term is recursively cumulated so that the order of the terms affects the symmetry value. Consequently, if two contours are dissimilar, then the error also accumulates over every succeeding term. Let  $\xi$  be the total magnitude deviation between each of the corresponding  $n$  terms of  $v^\alpha$  and  $v^\beta$  so that

$$\xi = \sum_{i=1}^n | \|v_i^\alpha\| - \|v_i^\beta\| |.$$

The method is more sensitive and likely to detect similar, but unsymmetrical contours. Thus, the symmetry values  $\delta$  calculated using global contour symmetry are significantly lower than the  $\delta$  values calculated with global signature symmetry and require a more stringent definition of symmetry. The discrepancy of  $\delta$  values is a result of comparing the distance versus curvature layout of a contour. The magnitude values calculated using global contour symmetry disregards the angular position of the point. Global signature symmetry provides a more stringent measure of symmetry because angular position is accounted. The nature of the signature curve parametrization encodes curvature, hence compares curvature instead of distance, as in global contour symmetry. However, both methods indicate that benign contours generally possess global symmetry.

In contrast, the local symmetry calculations indicate that malignant tumors have a significantly greater propensity to display local symmetry as opposed to global symmetry. From a biological perspective, systems seek to attain order, which is expressed by symmetry patterns within the system. However, natural order is attained at different levels based on cellular functionality within the tumor. Differing symmetry patterns distinguish benign versus malignant tumors, while reflecting the contrasting biological nature of the tumors. The global symmetry of benign tumors indicates a higher degree of cellular functionality, compared to the more dysfunctional malignant tumors. However, the signature curve of malignant tumor contours displays local symmetry caused by spiculation. The symmetry pattern reflects that natural systems seek order, but achieve order at different levels. Spiculation creates pockets of symmetry along the contour, which can be detected by local individual and joint symmetry patterns in the signature curve.

## 5. CONCLUSION

Signature curves precisely capture an object's shape in order to detect and quantify changes in curvature indistinguishable to the human eye. Oncology is a natural application for signature curves because a high degree of curvature complexity is strongly correlated with malignancy. Signature curves have proven especially effective as a means of detecting symmetry, especially local symmetry. In global contour symmetry, we have shown that signature curves are not necessary for detecting global symmetry. However, signature curves significantly reduce the computational complexity of automatic local symmetry detection [7]. Although our symmetry methodology has only been applied to breast tumors, the algorithm can also be used in a variety of computer vision applications as a means of quantifying global and local symmetry of arbitrary two and three dimensional objects [14, 15]. For example, we have adapted the symmetry algorithm as a similarity measure in order to solve spherical jigsaw puzzles [9]. In three dimensions, the distance, polar angle, and azimuthal angle are cumulated as a measure of similarity between edges' signature curves in order to find matching pieces. Although similarity and symmetry can be detected without the use of signature curves, the curvature parametrization accentuates symmetry patterns so that a comparison can be calculated in a computationally efficient manner.

## 6. ACKNOWLEDGEMENTS

This work was funded by a CSUMS grant number DMS0802959 from the National Science Foundation in collaboration with the University of St. Thomas. In addition, the author would like to thank Dr. Chehrzad Shakiban for advising the research which lead to this paper.

## REFERENCES

- [1] Boutin, M., Numerically invariant signature curves, *International Journal of Computer Vision* **40** (2014).
- [2] Calabi, E., Olver, P., Shakiban, C., Tannenbaum, A., and Haker, S., Differential and numerically invariant signature curves applied to object recognition, *Int. J. Computer Vision* **26** (1998).
- [3] Cartan, É., La méthode du repère mobile, la théorie des groupes continus, et les espaces généralisés, *Exposés de Géométrie* **5** (1937).
- [4] Cartan, É., La théorie des espaces, *Connexion Projective* **17** (1937).
- [5] Chen, D., Classification of breast ultrasound images using fractal feature, *Journal of Clinical Imaging* **29** (2005), 235-245.
- [6] DeBerardinis, R., The biology of cancer: metabolic reprogramming fuels cell growth and proliferation, *Cell metabolism* **7.1** (2008), 11-20.
- [7] Giblin, P., and Brassett, S., Local symmetry of plane curves, *The American Mathematical Monthly* **92.10** (1985), 689-707.
- [8] Gokhale, S., Ultrasound characterization of breast masses, *Indian Journal of Radiology and Imaging*, **242**.
- [9] Grim, A., O'Connor, T., Olver, P.J., Shakiban, C., Slechta, R., and Thompson, R., Reassembly of three-dimensional jigsaw puzzles, preprint, 2015.
- [10] Keller, M., Curvature, geometry and spectral properties of planar graphs, *Discrete and Computational Geometry*, **46.3** (2011), 500-525.
- [11] Lankton, S., Hybrid geodesic region-based curve evolutions for image segmentation, *Medical Imaging, International Society for Optics and Photonics* (2007).
- [12] Lankton, S., and Tannenbaum, A., Localizing region-based active contours, *Image Processing, IEEE Transactions* **17.11** (2008).
- [13] Lloyd, R., and Shakiban, C., Classification of signature curves using latent semantic analysis, *Computer Algebra and Geometry Algebra with Applications* **3519** (2005).
- [14] Martinet, A., Accurate detection of symmetries in 3d shapes, *ACM Transactions on Graphics* **25.2** (2006), 439-464.
- [15] Mitra, N., Guibas, L., and Pauly, M., Partial and approximate symmetry detection for 3D geometry, *ACM Transactions on Graphics* **25.3** (2006), 560-568.
- [16] Pohlman, S., Quantitative classification of breast tumors in digitized mammograms, *Medical Physics* **23.8** (1996): 1337-1345.
- [17] Rangayyan, R., Measures of acutance and shape for classification of breast tumors, *Medical Imaging, IEEE Transactions* **16.6** (1997), 799-810.
- [18] Rangayyan, R., and Nguyen, T., Fractal Analysis of Contours of Breast Masses in Mammograms, *Journal of Digital Imaging* **20.3** (2007), 223-237.
- [19] Suckling, J., (1994): The Mammographic Image Analysis Society Digital Mammogram Database Excerpta Medica. International Congress Series 1069.
- [20] Sulik, G., "Breast Cancer", *The Multimedia Encyclopedia of Women in Today's World*. Ed., SAGE Publications (2010).
- [21] University of South Florida, University of South Florida Digital Mammography Home Page, <http://marathon.csee.usf.edu/Mammography/Database.html>.
- [22] Vogelstein, B., and Kinzler, K., The multistep nature of cancer, *Trends in Genetics* **9.4** (1993), 138-141.

## STUDENT BIOGRAPHIES

**Anna Grim:** (*Corresponding author:* grim4684@stthomas.edu) Anna Grim will be a senior majoring in mathematics at the University of St. Thomas in 2015–2016. She plans to attend graduate school to pursue a Ph.D in applied mathematics with a concentration in mathematical biology and dynamical systems.